Single-photon side bands

T. C. Ralph,[1] E. H. Huntington,[2] and T. Symul[3]
[1]*Department of Physics, University of Queensland, Brisbane 4072, QLD, Australia*
[2]*Centre for Quantum Computer Technology, School of Information Technology and Electrical Engineering, University College, The University of New South Wales, Canberra, ACT, 2600 Australia*
[3]*Department of Physics, Faculty of Science, The Australian National University, Canberra, ACT, 0200 Australia*
(Received 31 December 2007; published 11 June 2008)

Single-photon states (and other non-Gaussian states) are typically studied in the time domain. In contrast, continuous-variable Gaussian states such as squeezed states are typically studied at side-band frequencies. Much of modern optical communication technology is also based on side-band techniques. Here we discuss what it means to produce single-photon states at side-band frequencies and propose techniques for producing and analyzing such states.

DOI: 10.1103/PhysRevA.77.063817 PACS number(s): 42.50.Dv

I. INTRODUCTION

Quantum optics used to be clearly divided into two camps: continuous variables and discrete variables [1]. Continuous-variable experiments measured the quadrature variables of the optical field at side-band frequencies using frequency resolved homodyne detection and typically employed "bright" light sources of a few milliwatts. Discrete-variable experiments measured the photon number in a particular time window using avalanche photodiodes and typically employed "weak" light sources of a few nanowatts.

Recently this divide has been bridged with several experiments combining photon counting and homodyne detection [2–6]. These experiments could be broadly characterized as working from the discrete-variable side, by introducing time domain homodyne techniques suitable for analyzing weak light sources. Here we wish to consider working more from the continuous-variable side by adapting our state preparation techniques to produce single-photon side-band states, potentially carried on bright light beams, that can be analyzed using frequency resolved homodyne techniques.

We begin in the next section by reviewing frequency resolved homodyne detection techniques and the nature of the side-band states it analyzes. In Sec. III, armed with this analysis, we consider examples of side-band states that would exhibit a single-photon homodyne signature. We find that the required states are equal superpositions of a single photon residing in the upper and lower side band. We also discuss a technique for the heralded production of such a state from a two-mode entangled state. This requires narrow optical filtering such that only a single side band falls on a trigger photon counter, and unitary frequency mixing of the heralded mode. Although challenging, these techniques are currently feasible.

In Sec. IV we show that if, for demonstration purposes, we are willing to forego single shot capabilities and focus only on ensemble measurements, then an experiment using Gaussian input states and no single-photon resolving measurements is possible. In this case both the trigger and heralded modes are detected with frequency resolving homodyne detection. This means no complicated optical filtering or manipulation is necessary. On the other hand the classical post processing of the signals is more involved. In Sec. V we conclude.

II. FREQUENCY RESOLVED HOMODYNE DETECTION

The observable measured by an ideal homodyne detector can be represented by the following Hermitian operator:

$$\hat{X}^{(\theta)}(t) = e^{-i\theta}\hat{a}(t) + e^{i\theta}\hat{a}^{\dagger}(t) = \int_{-\infty}^{\infty} d\omega e^{i\omega t}(e^{-i\theta}\hat{a}_{\omega} + e^{i\theta}\hat{a}^{\dagger}_{-\omega}), \tag{1}$$

where θ is the phase difference between the signal and the local oscillator and the frequencies ω are side-band frequencies above and below the optical frequency Ω. Strictly speaking the lower bound of the integral should be $-\Omega$ but for optical frequencies it is a good approximation to extend the lower bound to $-\infty$. Given this approximation the time domain $[\hat{a}(t)]$ and frequency domain $(\hat{a}_{\omega})$ annihilation operators and their Hermitian conjugates are Fourier transform pairs. We are particularly considering a situation here where the intrinsic time resolution of the detector is much narrower than typical field features, such that the frequency domain operators can be considered delta correlated, i.e., $[\hat{a}_{\omega}, \hat{a}^{\dagger}_{\omega'}] = \delta(\omega - \omega')$. Particular frequency side-band modes can be isolated by multiplying the homodyne signal by a cosine and doing a time integration (mixing down) giving

$$\hat{X}^{(\theta)}_{\omega_s} = \int dt \cos(\omega_s t + \phi)\hat{X}^{(\theta)}(t)$$
$$= \frac{1}{\sqrt{2}}(e^{-i(\theta+\phi)}\hat{a}_{\omega_s} + e^{i(\theta+\phi)}\hat{a}^{\dagger}_{\omega_s} + e^{-i(\theta-\phi)}\hat{a}_{-\omega_s} + e^{i(\theta-\phi)}\hat{a}^{\dagger}_{-\omega_s}), \tag{2}$$

where ϕ is the mix-down phase. We obtain a signal that contains equal contributions from the upper and lower side bands. In reality the cosine will have a finite spread in frequency and thus the mixed down signal will be a finite width side-band mode. We use the single frequency approximation for simplicity. This approximation is valid for spectral features that are slowly varying over the mix-down width.

For general side-band modes our detector will return a mixed result. However, for a particular class of symmetric side-band modes pure state statistics can be obtained. First suppose we have no phase reference for the side-band modes. This would be the situation if, for example, we fed our detected photocurrent directly into a spectrum analyzer. Effectively we are using a random ϕ for each shot. We model this by averaging over all ϕ. Clearly the first order moments are zero as

$$\int_0^{2\pi} d\phi \hat{X}_{\omega_s}^{(\theta)} = 0. \tag{3}$$

However, the second order moments are nonzero as we have

$$\frac{1}{2\pi}\int_0^{2\pi} d\phi (\hat{X}_{\omega_s}^{(\theta)})^2 = \frac{1}{2}(2e^{-i2\theta}\hat{a}_{\omega_s}a_{-\omega_s} + 2e^{i2\theta}\hat{a}_{-\omega_s}^{\dagger}\hat{a}_{\omega_s}^{\dagger} + \hat{a}_{-\omega_s}\hat{a}_{-\omega_s}^{\dagger} + \hat{a}_{-\omega_s}^{\dagger}\hat{a}_{-\omega_s} + \hat{a}_{\omega_s}\hat{a}_{\omega_s}^{\dagger} + \hat{a}_{\omega_s}^{\dagger}\hat{a}_{\omega_s}). \tag{4}$$

Now consider the state $\hat{U}|\psi\rangle_{\omega_s}|\psi'\rangle_{-\omega_s}$ where $|\psi\rangle$ is an arbitrary state, $|\psi'\rangle$ is a phase shifted version of this state, $|\psi'\rangle = \exp[i\pi/2\hat{a}^{\dagger}\hat{a}]|\psi\rangle$, and $\hat{U}$ is the frequency mixing unitary operator defined by $\hat{U}^{\dagger}\hat{a}_{\pm\omega}\hat{U} = 1/\sqrt{2}(\hat{a}_{\omega} \pm \hat{a}_{-\omega})$. From Eq. (4), the expectation value of the second moment at angle θ is given by

$$\begin{aligned}\langle(\hat{X}_{\omega_s}^{(\theta)})^2\rangle &= \langle\psi|_{\omega_s}\langle\psi|_{-\omega_s}\hat{U}^{\dagger}(\hat{X}_{\omega_s}^{(\theta)})^2\hat{U}|\psi\rangle_{\omega_s}|\psi'\rangle_{-\omega_s} \\ &= \frac{1}{2}[\langle\psi|_{\omega_s}(e^{-i\theta}\hat{a}_{\omega_s} + e^{i\theta}\hat{a}_{\omega_s}^{\dagger})^2|\psi\rangle_{\omega_s} \\ &\quad + \langle\psi|_{-\omega_s}(e^{-i\theta}\hat{a}_{-\omega_s} + e^{i\theta}\hat{a}_{-\omega_s}^{\dagger})^2|\psi\rangle_{-\omega_s}].\end{aligned} \tag{5}$$

As an example suppose we wish to observe statistics equivalent to a squeezed vacuum state $|S\rangle$. The required input state $\hat{U}|S\rangle_{\omega_s}|S'\rangle_{-\omega_s}$ is an Einstein, Podolsky, Rosen (EPR) or two-mode squeezed state between the two frequency modes. That entanglement exists between the side-band modes of typical squeezed states has been known for a long time [7] and was recently experimentally demonstrated [8].

If we have phase information about the side-band states then it is possible to lock to a particular mix-down phase [9]. Suppose we choose the mix-down phase $\phi=0$. Now we find that all order moments are accessible via

$$\langle(X_{\omega_s}^{(\theta)})^n\rangle = \langle\psi|_{\omega_s}(e^{-i\theta}\hat{a}_{\omega_s} + e^{i\theta}\hat{a}_{\omega_s}^{\dagger})^n|\psi\rangle_{\omega_s}. \tag{6}$$

Notice that now our homodyne signal only depends on the state of the upper side band (before frequency mixing), allowing us to relax the condition on the input state to be $\hat{U}|\psi\rangle_{\omega_s}|\phi\rangle_{-\omega_s}$, where now $|\psi\rangle_{\omega_s}$ and $|\phi\rangle_{-\omega_s}$ can be different arbitrary states. An example of this situation is if we want to observe statistics equivalent to a coherent state $|\alpha\rangle$. This means the required input state could be $\hat{U}|\alpha\rangle_{\omega_s}|0\rangle_{-\omega_s} = |1/\sqrt{2}\alpha\rangle_{\omega_s}|1/\sqrt{2}\alpha\rangle_{-\omega_s}$, as can be created via amplitude modulation. The mix-down angle would be locked to the phase of the signal generator driving the amplitude modulator.

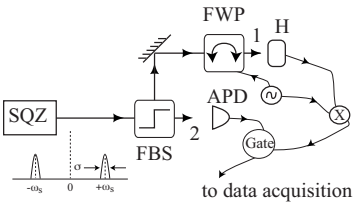

FIG. 1. Schematic of the scheme to achieve the desired input state. Here SQZ indicates a cavity based squeezer, FBS indicates a frequency beam splitter, FWP indicates a frequency wave plate, APD indicates an avalanche photodiode, and H indicates a homodyne detector.

III. SINGLE-PHOTON SIDE-BAND STATES

We now have the tools necessary to consider what type of states we need to create in order to observe single-photon statistics with frequency resolved homodyne detection. Consider first the case in which no mix-down phase is available. Directly generalizing our previous examples we conclude that the state

$$\hat{U}|1\rangle_{\omega_s}|1\rangle_{-\omega_s} = \frac{1}{\sqrt{2}}(|2\rangle_{\omega_s}|0\rangle_{-\omega_s} + |0\rangle_{\omega_s}|2\rangle_{-\omega_s}) \tag{7}$$

will display the required single-photon statistics. Equation (7) says that we require two photons to be present in order to observe single-photon statistics if no mix-down phase is available. Producing the state of Eq. (7) would be challenging hence we now consider the case where we are able to lock to a particular mix-down angle. In the previous section we showed that if we lock to $\phi=0$ then the homodyne signal only depends on the state of the upper side band before mixing. Thus we will obtain the desired statistics if our input state is given by

$$\hat{U}|1\rangle_{\omega_s}|0\rangle_{-\omega_s} = \frac{1}{\sqrt{2}}(|1\rangle_{\omega_s}|0\rangle_{-\omega_s} + |0\rangle_{\omega_s}|1\rangle_{-\omega_s}). \tag{8}$$

We now describe how to produce and lock to this state. Figure 1 illustrates the scheme. To first order the output state of a cavity based degenerate optical parametric amplifier (OPA) is

$$|\psi\rangle \approx |0\rangle + \int_{\infty}^{\infty} \Psi(\omega)|1\rangle_{\omega}|1\rangle_{-\omega}d\omega, \tag{9}$$

where the function $\Psi(\omega)$ takes account of the frequency dependence of the phase-matching function and the spectral filtering of the cavity and $\omega=0$ is the perfectly degenerate frequency. Physically, the OPA emits pairs of photons symmetrically spaced around the degenerate frequency. The magnitudes and relative phases of the two photons are given by the spectral function $\Psi(\omega)$. Here we are interested in pairs of photons emitted in a spectrum as indicated in Fig. 1. Such a spectrum could be achieved in a cavity based OPA with a combination of the cavity filter function and an additional

filter to inhibit the emission of pairs into higher-order longitudinal modes of the cavity. Again, for simplicity we consider first the idealized case where the filter function is delta correlated in frequency, i.e., $\Psi(\omega)=\delta(\omega-\omega_s)+\delta(\omega+\omega_s)$. The output of the squeezer under these conditions is given by $|\psi\rangle_{sqz}$ where

$$|\psi\rangle_{sqz} \approx |0\rangle + \chi|1\rangle_{\omega_s}|1\rangle_{-\omega_s}. \tag{10}$$

The pair of photons generated by the OPA are sent to a frequency-selective filter (denoted FBS in Fig. 1) that allows separation of the photons in the positive and negative side bands. An unbalanced Mach-Zehnder interferometer is explicitly modeled here but any high resolution filter would suffice for this application. The negative side-band output of this filter will be used to condition subsequent measurements via a broad-band avalanche photodiode. The frequency mixing operation is achieved via the device denoted FWP in Fig. 1. The FWP comprises another frequency selective filter combined with an acousto-optic modulator (AOM). This device, along with the frequency-selective filter, is discussed in more detail in Ref. [10]. A demonstration of quantum limited, coherent frequency mixing via this method can be found in Ref. [11]. The AOM is driven by a radio-frequency signal generator and has diffraction efficiency designed to give symmetric frequency mixing. The signal generator provides the radio-frequency phase reference for mix down. The state after interaction with this system is

$$|\psi\rangle_{out} \approx |0\rangle + \left[\frac{1}{\sqrt{2}}|1\rangle_{\omega_s}|0\rangle_{-\omega_s} + |0\rangle_{\omega_s}|1\rangle_{-\omega_s}\right]_1 \otimes |0\rangle_{\omega_s,2}|1\rangle_{-\omega_s,2}. \tag{11}$$

Triggering on detection of a single photon at output port 2 yields the state described by Eq. (8).

The state presented in Eq. (11) is unrealistic in that it assumes that the squeezer emits a single pair of single-frequency side bands. In reality the squeezer emits numerous pairs of side bands limited by the phase-matching bandwidth of the nonlinear crystal. Individual side-band pairs can be isolated by placing the squeezer in a suitable optical cavity or by subsequent cavity filtering. The thus selected side-bands will have some finite bandwidth, dictated by the cavity bandwidth and quantified by the variance σ, as indicated in the sketch in Fig. 1. The frequency-dependent components shown in Fig. 1 are optimized to work at the nominal frequencies $\pm\omega_s$, and so spectral components at other frequencies are not processed in quite the same way as one might desire. The effect of finite bandwidth can be quantified by evaluating the fidelity between the desired output state and the actual state. The results of calculations of this nature were presented in Ref. [10]. It suffices here to state that the fidelity depends very strongly on the ratio ω_s^2/σ. Fidelities of over 0.99 can be achieved with $\omega_s^2/\sigma=500$. These quantities are controlled by engineering the free spectral range (FSR) and linewidth of the squeezer cavity, respectively, and this ratio is fairly straightforward to achieve in practice. Finally, the homodyne detection system needs to be well matched to the projected single-photon state. This can be achieved by matching the spectral structure of the mix-down signal to the side-band characteristics and triggering it off avalanche photodiode (APD) counts [4,6].

IV. ENSEMBLE MEASUREMENTS OF SINGLE-PHOTON SIDE BANDS

It has been argued that photon number averages and strongly quantum mechanical signatures such as antibunching or violation of Bell inequalities, normally associated with photon counting measurements, can be observed using only homodyne detection [12]. The key property of these measures that makes this possible is that they are based on ensemble averages. Experiments demonstrating this technique have recently been published [13,14]. Here we propose an experiment that can measure the Wigner function of a postselected single-photon state from a two mode squeezer, even though no photon number resolving counter is present.

In the previous section we showed how to engineer the frequency structure of a postselected state so that it is consistent with frequency resolved homodyne detection. In this section we will sidestep this problem by making all our measurements using a frequency resolved homodyne. We will consider measurements and manipulations of squeezed states produced by an OPA. The output of the OPA [see Eq. (9)] has the right frequency correlations such that specific side-band modes are given (in the nomenclature of Sec. II) by $\hat{U}|S\rangle_{\omega_s}|S'\rangle_{-\omega_s}$. As shown in Sec. II, these states appear as single mode squeezed states to frequency resolved homodyne, with locked mix down at frequency ω_s. Thus in this section we are able to suppress the frequency structure of the squeezed states and simply write $\hat{U}|S\rangle_{\omega_s}|S'\rangle_{-\omega_s} \equiv |S(r,\epsilon)\rangle$ with r the squeezing parameter and ϵ the squeezing phase at side-band frequencies $\pm\omega_s$. An experimental implementation of this proposal would not require the frequency wave plates or optical filtering of the previous section and could rely simply on the homodyne detection and mix down to isolate the side-band modes of interest.

The postselection of a single-photon state from a two mode squeezed state, as first demonstrated by Lvovsky *et al.* [2], proceeds as shown diagrammatically in Fig. 2(a). The squeezer (or as it is often called in this situation, down converter) is run at low conversion efficiency such that with high probability either vacuum or a pair of photons is produced in any particular shot. A photon counter is placed at one output (state preparation) and a time resolved homodyne detector is placed at the other (state measurement). If the photon counter registers a photon then there is a high probability that a single photon is present in the other arm. The homodyne detector is conditionally activated on the basis of a count being observed and thus observes only these single-photon events. If the probability distribution of the homodyne observable $\hat{X}_b^{(\theta)}$ is observed for a sufficient range of θ's then a tomographic reconstruction of the single-photon state can be obtained. Obtaining such a reconstruction would appear to rely crucially on being able to select only the single-photon events using a single-photon counter. We will now show that this is not the case.

First notice that the probability distribution for the observable $\hat{X}_b^{(\theta)}$ can be constructed from the average values of the

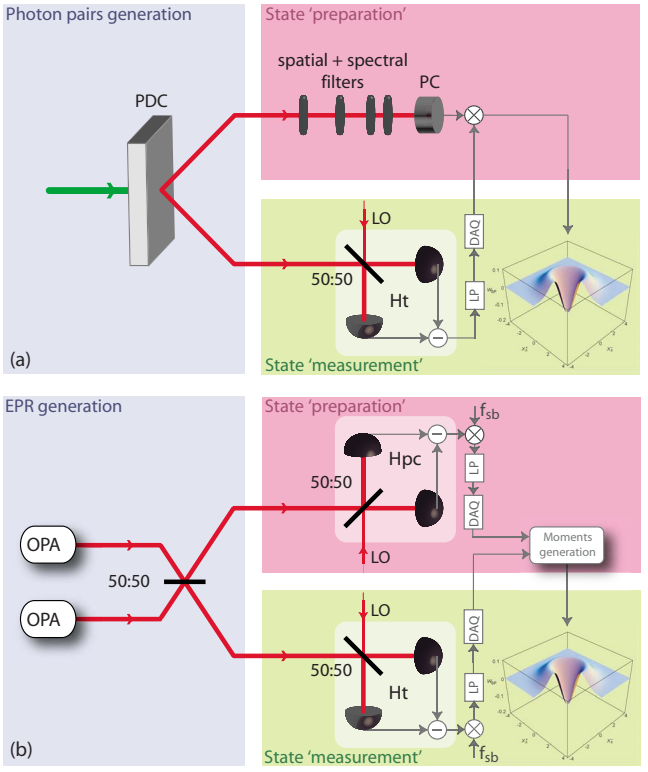

FIG. 2. (Color online) Schematic of the Fock state preparation scheme in (a) hybrid discrete-variable (DV)/CV regime and (b) CV regime. PDC: parametric down-converter; PC: photon counter (avalanche photodetector); 50:50: beam splitter; Ht: homodyne tomographic detector; LO: local oscillator reference beam; LP: low pass filter; DAQ: data acquisition; OPA: optical parametric amplifier (squeezing source); Hpc: homodyne photon counter, f_{sb}: side-band reference frequency.

moments of the observable, i.e., $\langle \hat{X}_b^{(\theta)} \rangle, \langle (\hat{X}_b^{(\theta)})^2 \rangle, \langle (\hat{X}_b^{(\theta)})^3 \rangle \ldots$. Second, notice that these moments can be obtained conditionally via the correlation moments $\langle \hat{n}_a \hat{X}_b^{(\theta)} \rangle, \langle \hat{n}_a (\hat{X}_b^{(\theta)})^2 \rangle, \langle \hat{n}_a (\hat{X}_b^{(\theta)})^3 \rangle \ldots$, where $\hat{n}_a$ is the operator describing the photon number observable of the state preparation mode. These correlation moments would be obtained by raising the output data of the homodyne detector to the required order but then multiplying shot by shot by the output data of the single-photon counter before averaging. The relevant eigenvalues of $\hat{n}_a$ are 0 and 1. When 0 is obtained the corresponding piece of homodyne data does not contribute to the average, however, when 1 is obtained the corresponding data does contribute. Hence only the data corresponding to times when the photon counter fired is kept. The moments thus obtained will be scaled by a constant representing the probability of success. Knowing this probability allows the moments to be renormalized.

So far we have discussed how the tomographic reconstruction of conditional single-photon states from a two-mode squeezed state can be recast as a correlation experiment between single-photon counts on one arm of the entangled state and homodyne measurements on the other. Now we show that the problem can be further recast into a correlation experiment involving only homodyne measurements [see Fig. 2(b)]. The strategy is to use the operator equivalence $\hat{n} = 1/4[(\hat{X}^+)^2 + (\hat{X}^-)^2 - 2]$ to turn number–homodyne correlations into homodyne–homodyne correlations [12]. Here we have used the notation $\hat{X}^+ = \hat{X}^{(0)}$ for the in-phase quadrature and $\hat{X}^- = \hat{X}^{(\pi/2)}$ for the out-of-phase quadrature. Thus the correlation moments we need to evaluate are

$$\begin{aligned} C_n^{(\theta)} &= \langle \hat{n}_a (\hat{X}_b^{(\theta)})^n \rangle \\ &= \langle \{1/4[(\hat{X}_a^+)^2 + (\hat{X}_a^-)^2 - 2]\} (\hat{X}_b^{(\theta)})^n \rangle \\ &= 1/4[\langle ((\hat{X}_a^+)^2 (\hat{X}_b^{(\theta)})^n \rangle + \langle ((\hat{X}_a^-)^2 (\hat{X}_b^{(\theta)})^n \rangle - 2\langle (\hat{X}_b^{(\theta)})^n \rangle]. \end{aligned} \tag{12}$$

Notice particularly that the expectation values factor into a sum of easily measured correlation products.

Let us now apply this method to a pair of spatially nondegenerate EPR beams. We will first illustrate how a weakly entangled beam behaves similarly to a pair of single photons. In the continuous-variable regime, a pair of EPR beams is conveniently created by mixing two squeezed beams in quadrature on a beam splitter [see Fig. 2(b)]. The EPR beam can therefore be expressed as [1]

$$|\mathrm{EPR}\rangle_{a,b} = \mathrm{BS}|S(r,0)\rangle|S(r,\pi/2)\rangle \tag{13}$$

where the beam splitter operator acting on Fock states can be expressed as

$$\begin{aligned} \widehat{\mathrm{BS}}|m\rangle|n\rangle = \frac{1}{\sqrt{2^{m+n}}} \sum_{j,k=0}^{j=m,k=n} \frac{\sqrt{m!\,n!\,(m+n-j-k)!\,(j+k)!}}{j!\,k!\,(m-j)!\,(n-k)!} \\ \times (-1)^k |m+n-j-k\rangle|j+k\rangle \end{aligned} \tag{14}$$

and the Schmidt decomposition of the squeezed states is given by

$$|S(r,\epsilon)\rangle = \sqrt{\mathrm{sech}(r)} \sum_{n=0}^{\infty} \frac{\sqrt{(2n)!}}{n!} [-1/2 e^{i\epsilon} \tanh(r)]^n |2n\rangle, \tag{15}$$

where $r = -\frac{1}{2}\ln(V_s)$ is the squeezing parameter with V_s being the variance of the squeezed quadrature normalized to the quantum noise. Therefore the well known Schmidt decomposition of the EPR beam is given by

$$|\mathrm{EPR}\rangle_{a,b} = \mathrm{sech}(r) \sum_{n=0}^{\infty} [-\tanh(r)]^n |n\rangle_a |n\rangle_b. \tag{16}$$

We can see that for small entanglement, i.e., small value of squeezing ($V_s \approx 1$), only the first two order terms are significant:

$$|\mathrm{EPR}\rangle_{a,b} = |0\rangle_a|0\rangle_b + r|1\rangle_a|1\rangle_b. \tag{17}$$

Using the previous equation, it is easy to show that

$$\frac{\langle \mathrm{EPR}|\hat{n}_a(\hat{X}_b^{(\theta)})^n|\mathrm{EPR}\rangle}{\langle \mathrm{EPR}|\hat{n}_a(\hat{X}_b^{(\theta)})^0|\mathrm{EPR}\rangle} = [1+(-1)^n]\frac{\prod_{i=1}^{n/2} 1+2i}{2^{n/2}} = \langle 1|(X^{(\theta)})^n|1\rangle \tag{18}$$

and thus the probability distribution reconstructed from these moments will be that of a single-photon state. We now show explicitly that the same result can be obtained directly from the quadrature correlations. We begin by rewriting Eq. (12) as

$$C_n^{(\theta)} = D_n^{(\theta)} - 1/2\langle(\hat{X}_b^{(\theta)})^n\rangle, \tag{19}$$

where $D_n^{(\theta)} = 1/4[\langle(\hat{X}_a^+)^2(\hat{X}_b^{(\theta)})^n\rangle + \langle(\hat{X}_a^-)^2(\hat{X}_b^{(\theta)})^n\rangle]$. Because of the symmetry of the EPR state with respect both to spatial modes and quadrature angle and the Gaussian nature of the quadrature moments we have

$$\langle(\hat{X}_a^{\theta})^n\rangle = \langle(\hat{X}_b^{\theta})^n\rangle \approx \prod_{k=1}^{n/2}(2k-1)(1+n/2r^2) \tag{20}$$

for n even, where again we take $r \ll 1$. For n odd the moments are all zero. Similarly evaluating the correlation moments to second order in r we find

$$D_0^{(\theta)} \approx (1+r^2),$$

$$D_2^{(\theta)} \approx (1+r^2)(1+3r^2),$$

$$D_4^{(\theta)} \approx (1+r^2)3(1+6r^2),$$

$$D_6^{(\theta)} \approx (1+r^2)15(1+9r^2)\ldots, \tag{21}$$

where again all odd order moments are zero. We recognize Eq. (21) as an unnormalized Gaussian distribution with variance $(1+3r^2)$. Thus we conclude that the probability distribution corresponding to the moments of Eq. (12) is given by the difference of two Gaussians,

$$P^{\theta}(x) \approx \frac{1}{\sqrt{2\pi}}\left(\frac{1+r^2}{\sqrt{1+3r^2}}e^{-x^2/1+3r^2} - \frac{1}{\sqrt{1+r^2}}e^{-x^2/1+r^2}\right) \approx \frac{1}{\sqrt{2\pi}}2r^2x^2e^{-x^2} \tag{22}$$

with $x \equiv X_b^{\theta}$. When normalized against the probability of obtaining a coincidence, r^2, the last line of Eq. (22) corresponds to the quadrature probability distribution of a single-photon state, thus completing our proof.

We now seek an exact solution. Evaluating the influence of further terms in the Schmidt decomposition of the EPR beams, however, becomes quickly complicated as it involves evaluating all the nonzero contributions of the development of $(\hat{X}_b^{(\theta)})^n = (e^{i\theta}\hat{b} + e^{-i\theta}\hat{b}^{\dagger})^n$. One can see that in this development, only the terms comprising the same amount of operators $\hat{b}$ and $\hat{b}^{\dagger}$ will give nonzero values. This shows that all the odd order moments are zero, and that the final result is independent of θ, but it still leaves $\frac{n!}{(n/2)!^2}$ terms to evaluate for the nth order moment. Although maybe less intuitive, it is therefore more appropriate to use the Wigner representation of the EPR state to calculate the moments. The Wigner representation of the EPR state is given by the four dimension formula:

$$W_{\mathrm{EPR}}(X_a^+, X_b^+, X_a^-, X_b^-) = \frac{1}{4\pi^2}e^{2(1-V_s^2)/4V_s(X_a^+X_b^+ - X_a^-X_b^-)} \times e^{-(V_s^2+1)/4V_s[(X_a^+)^2+(X_a^-)^2+(X_b^+)^2+(X_b^-)^2]}. \tag{23}$$

We first perform the changes of variables $X_b^+ = X_b^{\theta}\cos\theta - X^{\theta+\pi/2}\sin\theta$, and $X_b^- = X_b^{\theta}\sin\theta + X^{\theta+\pi/2}\cos\theta$ to obtain $W_{\mathrm{EPR}}(X_a^+, X_b^{\theta}, X_a^-, X_b^{\theta+\pi/2})$. We note that W_{EPR} (being the Wigner function of a Gaussians state) is always positive and can be interpreted as a probability distribution of continuous-variable (CV) measurements. Therefore by noticing that the mean value of the function $f(x)$ of a random variable x with probability distribution, $P(x)$ is given by $\langle f(x)\rangle = \int_{-\infty}^{\infty} f(x)P(x)dx$, Eq. (12) can be rewritten as

$$C_n^{(\theta)} = \frac{1}{4}\int\int\int\int_{-\infty}^{\infty}[(X_a^+)^2(X_b^{\theta})^n + (X_a^-)^2(X_b^{\theta})^n - 2(X_b^{\theta})^n]W_{\mathrm{EPR}}(X_a^+, X_b^{\theta}, X_a^-, X_b^{\theta+\pi/2})dX_a^+dX_b^{\theta}dX_a^-dX_b^{\theta+\pi/2}, \tag{24}$$

$$= \frac{[1+(-1)^n]}{16\sqrt{\pi}}\left[V_s^{(n/2)-1}(V_s^2+1)^{n/2-1}[n(V_s^2-1)^2 + 2(V_s^2+1)^2] - 4\left(\frac{V_s}{V_s^2+1}\right)^{-n/2}\right]\Gamma\left(\frac{n+1}{2}\right) \tag{25}$$

which confirms that the moments are independent of θ and that the odd nth order moments are zero.

Now that we know all the moments $C_n^{(\theta)}$, the Wigner function $W_{\mathrm{SP}}(X_b^{\theta})$, and the probability distributions, of the observable $\hat{X}_b^{\theta}$ conditioned on $\hat{n}_a$, can be calculated by noticing that the characteristic function (i.e., Fourier transform) $\Phi(\nu_b^{\theta})$ of the probability distribution $P(X_b^{\theta})$ can be expressed as a Taylor series:

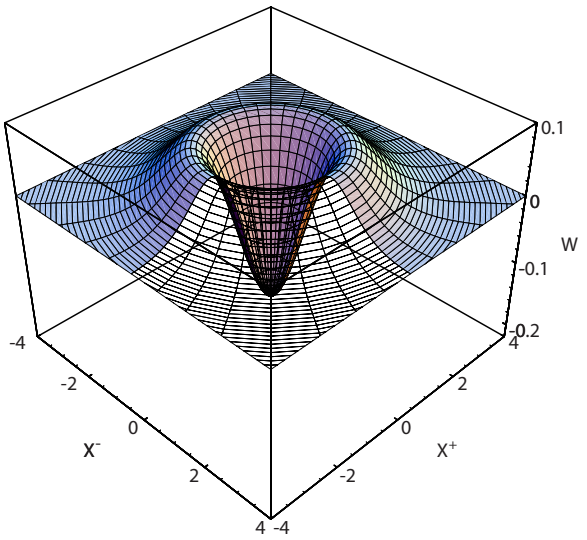

FIG. 3. (Color online) Reconstructed theoretical Wigner function for $V_s=0.8(\approx -2$ dB).

$$\Phi(\nu_b^\theta)=\sum_{n=0}^{\infty}\frac{i^n(\nu_b^\theta)^n}{n!}C_n^{(\theta)} \tag{26}$$

then, using the central slice theorem, the Fourier transform $F(\nu_x,\nu_y)$ of $W_{\mathrm{SP}}(X_b^\theta)$ can be calculated as

$$F(\nu_x,\nu_y)=\Phi\left[\sqrt{\nu_x^2+\nu_{y_b}^2}\tan^{-1}(\nu_y/\nu_x)\right]. \tag{27}$$

One should note that due to the fact that the characteristic function $\Phi(\nu_b^\theta)$ is expressed as a Taylor series, it will diverge toward infinity when calculated only up to a limited order. This problem can be overcome by padding $\Phi(\nu_b^\theta)$ with 0 for big values of ν_b^θ, discretizing it, and then making use of discrete Fourier transforms to reconstruct the Wigner function $W_{\mathrm{SP}}(X_b^\theta)$.

Figure 3 shows a three-dimensional (3D) representation of $W_{\mathrm{SP}}(X_b^\theta)$ for $V_s=0.8$. As expected for this small value of squeezing the Wigner function clearly dips below zero. Figure 4 represents cuts through the center of the Wigner function, and shows how $W_{\mathrm{SP}}(X_b^\theta)$ evolves as the squeezing increases. As expected from Eq. (18), for the small value of squeezing the Wigner function is very similar to the one of a single photon. When the squeezing increases contributions from higher photon numbers become significant, the Wigner function starts spreading, and the negative region decreases but stays present.

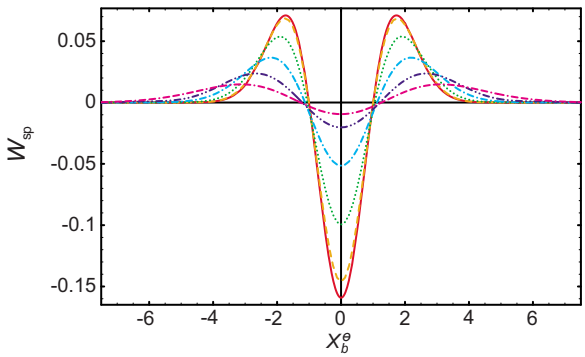

FIG. 4. (Color online) Cuts through the center of the Wigner functions $W_{\mathrm{SP}}(X_b^\theta)$ for varying value of squeezing. (solid) single photon using the moment definition given by Eq. (18), (dash) $V_s=-1$ dB, (dot) $V_s=-3$ dB, (dash-dot) $V_s=-5$ dB, (dash-dot-dot) $V_s=-7$ dB, and (dash-dash-dot) $V_s=-9$ dB.

V. CONCLUSION

We have discussed the characteristics of single-photon states needed such that they may be observed via frequency resolved homodyne detection at side-band frequencies. A motivation for looking at such states is that they may allow multiplexing of many single-photon states on a single spatial mode. We examined two approaches to observing these states. The first is a single shot method that can herald a single photon in a side-band frequency state compatible with frequency resolved homodyne. The second is an ensemble approach that enables tomography of a postselected single-photon side-band state. A unique feature of the second approach is that no single-photon resolving measurements are required.

Although we have restricted our attention here to single-photon states the general arguments could be extended to more general non-Gaussian states such as macroscopic quantum superposition (so-called "cat") states [15] or Gottesman-Kitaev-Preskill (GKP) states [16]. Such states, along with single-photon states, may play important roles in future quantum communication and processing systems that may benefit from the techniques outlined here.

ACKNOWLEDGMENTS

We thank Ping Koy Lam and Philippe Grangier for useful discussions. This work was supported by the Australian Research Council and the Defence Science Technology Organization.

[1] H.-A. Bachor and T. C. Ralph, *A Guide to Experiments in Quantum Optics*, 2nd ed. (Wiley-VCH, Weinheim, 2004).
[2] A. I. Lvovsky, H. Hansen, T. Aichele, O. Benson, J. Mlynek, and S. Schiller, Phys. Rev. Lett. **87**, 050402 (2001).
[3] A. Ourjoumtsev, R. Tualle-Brouri, J. Laurat, and P. Grangier, Science **312**, 83 (2006).
[4] J. S. Neergaard-Nielsen, B. M. Nielsen, C. Hettich, K. Molmer, and E. S. Polzik, Phys. Rev. Lett. **97**, 083604 (2006).
[5] A. Ourjoumtsev, H. Jeong, R. Tualle-Brouri, and P. Grangier, Nature (London) **448**, 784 (2007).
[6] K. Wakui, H. Takahashi, A. Furusawa, and M. Sasaki, Opt. Express **15**, 3568 (2007).
[7] C. M. Caves, Phys. Rev. D **26**, 1817 (1982); J. Gea-Banacloche and G. Leuchs, J. Mod. Opt. **34**, 793 (1987).

[8] E. H. Huntington, G. N. Milford, C. Robilliard, T. C. Ralph, O. Glockl, U. L. Andersen, S. Lorenz, and G. Leuchs, Phys. Rev. A **71** 041802(R) (2005).
[9] G. Breitenbach and S. Schiller, Nature (London) **387**, 471 (1997).
[10] E. H. Huntington and T. C. Ralph, Phys. Rev. A **69**, 042318 (2004).
[11] E. H. Huntington, G. N. Milford, C. Robilliard, and T. C. Ralph, Opt. Lett. **30**, 2481 (2005).
[12] T. C. Ralph, W. J. Munro, and R. E. S. Polkinghorne, Phys. Rev. Lett. **85**, 2035 (2000).
[13] J. G. Webb, T. C. Ralph, and E. H. Huntington, Phys. Rev. A **73**, 033808 (2006).
[14] N. B. Grosse, T. Symul, M. Stobinska, T. C. Ralph, and P. K. Lam, Phys. Rev. Lett. **98**, 153603 (2007).
[15] T. C. Ralph, A. Gilchrist, G. J. Milburn, W. J. Munro, and S. Glancy, Phys. Rev. A **68**, 042319 (2003).
[16] D. Gottesman, A. Kitaev, and J. Preskill, Phys. Rev. A **64**, 012310 (2001).